



Electrodeposition of copper-doped SnS thin films and their electric transmission properties control for thermoelectric enhancement

Ying Liu¹ · Kai Cao¹ · Jingjun Liu¹ · Zhengping Zhang¹ · Jing Ji¹ · Feng Wang¹ · Zhilin Li¹

Received: 18 June 2019 / Accepted: 23 July 2019 / Published online: 10 August 2019
© Springer Science+Business Media, LLC, part of Springer Nature 2019

Abstract

The thermoelectric performances of SnS are gradually noticed because of its structure similarity to SnSe which has the highest known thermoelectric performance. But the low electric transmission properties of SnS confines its thermoelectric performances. In this paper, we prepared Cu-doped SnS thin films with electrodeposition method. The Cu-doping content of the thin films were controlled by the adjustment of the electrolyte composition. The Cu doping narrowed the band gap of the SnS thin films, so that it promoted the carrier concentration of the films. The largest carrier concentration increased from 4.26×10^{15} to $436.42 \times 10^{15} \text{ cm}^{-3}$ after the Cu doping. By the additives in the electrolyte, the texture orientation and its coefficient were successfully controlled. The texture of (040) and (200) were obtained by the addition of urea and CTAB, respectively. The carrier mobility of the Cu-doped SnS thin films increased from 0.63 to 1.94 $\text{cm}^2/\text{V s}$ by the (200) texture. With a sample electrodeposition method, we successfully accomplished the combination of the Cu-doping and texture control of SnS thin films. Such a combination decreased the resistivity of the Cu-doped thin film with (200) texture from 322.53 to 24.50 $\Omega \text{ cm}$, so it was an effective path to improve the electric transmission performance of SnS thin films. Our results provide an easy method and a new view to improve the electric transmission performance of thermoelectric thin films.

1 Introduction

At present, large amount of energy is eventually wasted in the form of residual heat. Reuse of waste heat is one of the research hotspots of energy conservation. Thermoelectric materials have noticeable Seebeck effect by which waste heat can be directly converted into electricity [1]. Thermoelectric property of materials is normally judged by thermoelectric figure of merit $ZT = S\sigma^2T/\kappa$, where S , σ , T and κ represent the Seebeck coefficient, the electrical conductivity, the absolute temperature, and the thermal conductivity, respectively. Zhao et al. discovered that SnSe single crystal has ultra-low thermal conductivity along the b -axis because of its special twisted NaCl crystal structure. The ZT value

along b axis reached as high as 2.6 which is the highest known value [2–4]. So single crystal SnSe is regarded as the most hopeful thermoelectric material for commercial application. However, single crystal SnSe is difficult to prepare and its mechanical properties is disadvantageous for deformation processing. Moreover, the high price and toxicity of Se element are other shortcomings for commercial application. Development of substitutional materials is another path to solve the problems.

Tin monosulfide (SnS) is a IV–VI layered compound which possesses the same distorted NaCl type orthorhombic structure as that of SnSe [5]. So it can be supposed that SnS should also have high thermoelectric properties. However, the experiment ZT value of pure SnS is far smaller than applicable ones [6]. One of the reason is its low electric conductivity because of the low carrier concentration. It is reported that the carrier concentration of thermoelectric materials with large ZT value possess the carrier concentration range from 10^{19} to 10^{21} cm^{-3} [7, 8]. The carrier concentration of SnS is only 10^{15} cm^{-3} and its mobility is also low, which cause the low electric conductivity and low ZT value [9]. Therefore, in order to improve the thermoelectric properties of SnS, it is necessary to increase its carrier concentration and mobility [10–12], so as to reduce its resistivity.

✉ Feng Wang
wangf@mail.buct.edu.cn

✉ Zhilin Li
lizl@mail.buct.edu.cn

¹ State Key Laboratory of Chemical Resource Engineering, Beijing Key Laboratory of Electrochemical Process and Technology for Materials, Beijing University of Chemical Technology, Beijing 100029, People's Republic of China

Doping is an effective method to increase carrier concentration because the doping atoms can increase the number of carriers by accepting or supplying electrons [13]. The band gap of the intrinsic semiconductor can be narrowed by the donor level or the acceptor level provided by the doping atom, which facilitates the carrier excitation [14, 15]. As for the doping elements, all Cu [16], Na [17] and Ag [18, 19] were reported for SnS. It was proved that Na doping improves the thermoelectric properties effectively [15], but the doping process is difficult. Theoretical calculation indicated that Ag doping can also increase the carrier concentration of SnS [20–22], but Ag was too expensive for commercial application. Cu is far cheaper than Ag and was successfully doped into SnS by magnetron sputtering to form p-type SnS [23].

However, theoretical calculations indicated that the highest ZT value of SnS is only 0.6 at 750 K after p-type doping [6]. The low ZT value might be attributed to the carrier scattering occurs at the grain boundary which reduces the carrier mobility. Such carrier scattering might be reduced at certain preferential orientations to increase the carrier mobility and further improve the electric conductivity. Therefore, the preparation of the doping SnS with certain preferential orientations might be an effective path to compensate its low carrier concentration.

Compared with the preparation methods of physical vapor deposition [24], chemical vapor deposition [25], magnetron sputtering [23], sol–gel process [26] and thermal evaporation [27] for doping films, electrodeposition has the characters of simple processes and equipment requirements, low cost and easy commercialization [28]. Furthermore, the reduction potential of copper is close to that of Sn, so the doping of Cu into SnS should be easy to control by electrodeposition [29]. Some additives, such as urea and cetyltrimethylammonium bromide (CTAB) were proved facilitating the crystal growth on certain preferential orientations during electrodeposition [30, 31]. So the expected preferential orientations might be controlled by the adjustment of additives in the electrolytes.

In this work, we managed to increase the carrier concentrations of SnS thin films by Cu doping with electrodeposition, and increase the carrier mobility by the texture control of the thin films [32]. As a result, the electric conductivity is promoted in order to promote the thermoelectric performance of SnS thin films [33].

2 Experimental

2.1 Preparation of SnS thin films

In a three-electrode system, the auxiliary electrode was a platinum plate and the reference electrode was a saturated calomel electrode (SCE). The working electrode was

indium-tin oxide (ITO) covered glass with a deposition area of $2 \times 2 \text{ cm}^2$. The substrates were first cleaned with acetone, ethanol and deionized water orderly for 20 min, and then dried under nitrogen flow.

The electrolytic bath was consisted of 2 mM SnCl_2 , 10 mM $\text{Na}_2\text{S}_2\text{O}_3$ and 6 mM $\text{K}_4\text{O}_2\text{P}_7$. In order to adjust the texture, 0–15 mg/L urea and 0–15 mg/L CTAB were added into the electrolyte, respectively. The pH was adjusted around 3.0 using H_2SO_4 . A potential of -1.0 V (vs. SCE) was applied, and the deposition was performed at $50 \text{ }^\circ\text{C}$ for 40 min. After the electrodeposition, the as-deposited thin films were annealed at $350 \text{ }^\circ\text{C}$ for 0.5 h in a tube furnace with the protection of Ar flow.

2.2 Synthesis of Cu doped SnS thin films

On the basis of the electrolyte for SnS thin films, different amount of 5 mM CuCl_2 solution was added to reach the CuCl_2 content of 0.00625 mM, 0.0125 mM, 0.025 mM, 0.05 mM, respectively. The pH value of the solutions was adjusted to 2.8 with H_2SO_4 . A potential of -1.1 V (vs. SCE) was applied, and the deposition was still performed at $50 \text{ }^\circ\text{C}$ for 40 min. To adjust the texture of the Cu doped SnS thin films, various amounts of urea and CTAB were added, respectively. After the electrodeposition, the as-deposited Cu-doped SnS thin films were also annealed at $350 \text{ }^\circ\text{C}$ for 0.5 h under the protection of Ar flow.

2.3 Characterization of the thin films

To identify the crystal structure and the texture of the annealed thin films, X-ray diffraction (XRD) spectra were measured by an X-ray diffractometer (RINT 2200 V/PC) with Cu K_α radiation ($\lambda = 0.15406 \text{ nm}$) at 40 kV and 30 mA. A scanning electron microscope (SEM, JEOL FE-JSM-6701F, Japan) was used to observe the morphology of the thin films. Chemical compositions of the thin films were investigated by an energy dispersive X-ray (EDX) analyser (Oxford INCA-Penta-FET-X3, England), which is attached to the SEM equipment. Transmittance spectra were recorded by a UV–Vis spectrophotometer (Shimadzu UV-2450, Japan) in the wavelength range of 350–900 nm. According to the transmittance data, optical band gap E_g of the thin films was evaluated with the Tauc equation $(\alpha h\nu)^2 = A(h\nu - E_g)$ [34]. The electronic properties, including carrier type, concentration, and mobility were tested by a Hall effect measurement system (Phys. Tech. RH2030). The thin films were mechanically peeled off the substrates with marble glue before the Hall effect measurements.

Table 1 EDX results of SnS thin films deposited in different CTAB contents

CTAB content (mg/L)	Composition (at.%)		Atomic ratio Sn:S
	Sn	S	
0	49.89 ± 2.01	50.11 ± 2.01	1:1.00
2.5	49.96 ± 1.91	50.04 ± 1.91	1:1.00
5	51.92 ± 1.68	48.08 ± 1.68	1:0.93
10	52.61 ± 1.84	47.39 ± 1.84	1:0.90
15	51.69 ± 1.01	48.31 ± 1.01	1:0.93

Table 2 EDX results of SnS thin films deposited in different urea contents

CTAB content (mg/L)	Composition (at.%)		Atomic ratio Sn:S
	Sn	S	
2.5	51.69 ± 1.81	48.31 ± 1.81	1:0.93
5	50.98 ± 1.44	49.02 ± 1.44	1:0.96
10	51.46 ± 1.35	48.54 ± 1.35	1:0.94
15	48.98 ± 1.12	51.02 ± 1.12	1:1.04

3 Results and discussion

3.1 Structure analysis of SnS thin films

The composition of the SnS thin films deposited in electrolytes with different additives are shown in Tables 1, 2, respectively. It can be seen that the composition of the SnS thin films deposited without additives is quite closed to the stoichiometry. After the addition of CTAB or urea, the composition of the SnS thin films changed little, which is also closed to the stoichiometry. Therefore the orthogonal structure of SnS might be sustained for the thin films.

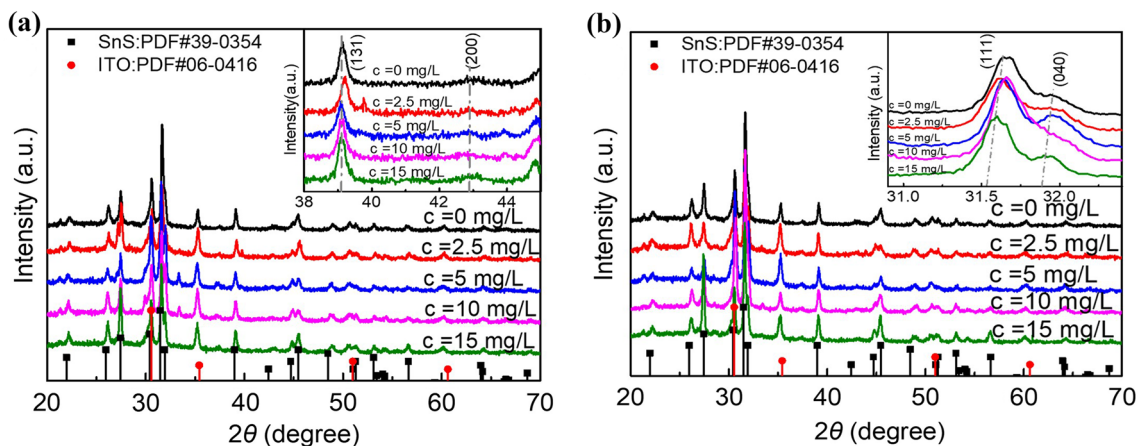
Figure 1 shows the XRD spectra of the SnS thin films deposited in different electrolytes. All diffraction peaks of (110), (120), (021), (111), (040), (131), (200), (141), (002), (151), (122), (042) of orthogonal SnS (JCPDS Cards 39-0354) appear. No other diffraction peaks can be observed except those of ITO substrate. So the structure of the thin films is pure orthogonal SnS. Additives seems to have no influence on the crystal structure of the thin films.

However, considering the texture of SnS thin films, different conclusions can be drawn. We calculated the texture coefficients of the SnS in different crystal orientations with the formula [35]:

$$T_{hkl} = \frac{I_{hkl}/I_{hkl}^0}{\frac{1}{n} \sum_{i=1}^n I_{HKL}/I_{HKL}^0} \quad (1)$$

where I_{HKL} represents the tested relative strength of the diffraction peak of any (HKL) crystal plane, I_{HKL}^0 represents the standard relative strength of the diffraction peak of the same (HKL) crystal plane, I_{hkl} represents the tested relative strength of the diffraction peak of the considering (hkl) crystal plane, I_{hkl}^0 represents the standard relative strength of the diffraction peak of the same (hkl) crystal plane, and n represents the total number of reflections. In our case, $n = 12$. And we calculated the texture coefficient of (200), (040), and (002) crystal planes, the results are shown in Fig. 2.

Figure 2a shows that the addition of CTAB caused obvious (200) and (040) textures, and the texture coefficient of (200) was larger than that of (040) normally. When the CTAB content reached 10 mg/L, the texture coefficient of (200) crystal plane reached as large as 2.32, so CTAB is an effective additive to form the texture of a -axis. Figure 2b shows that the addition of urea caused strong (040) texture and weak (002) texture. When the urea content reached 10 mg/L, the texture coefficient of (040) crystal plane

**Fig. 1** XRD spectra of the SnS thin films deposited in **a** different CTAB contents and **b** different urea contents

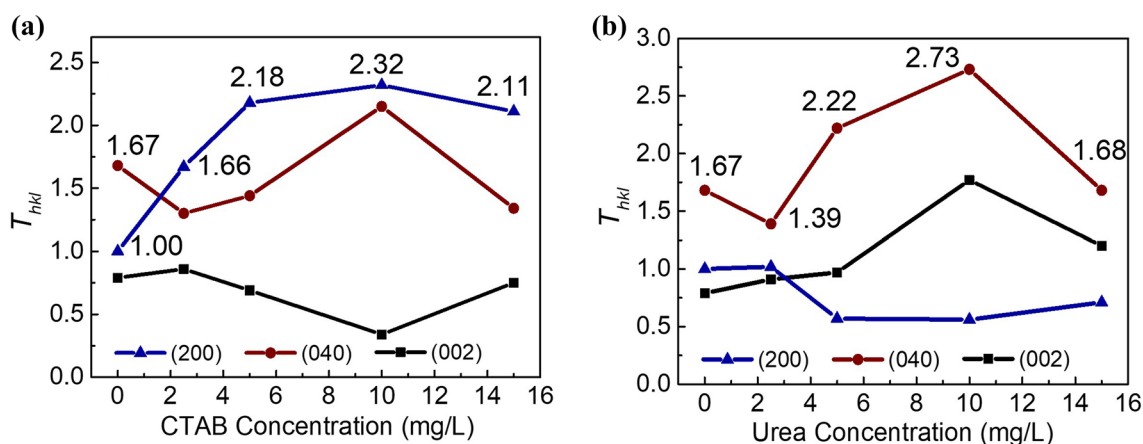


Fig. 2 Texture coefficient of the SnS thin films deposited in **a** different CTAB contents and **b** different urea contents

reached as large as 2.73, so urea is an effective additive to form the texture of *b*-axis. Therefore, the texture of the SnS thin films was successfully controlled by the adjustment of additives.

3.2 Composition, structure and electrical properties of Cu-doped SnS thin films

On the basis of the electrodeposition of SnS thin films, different contents of Cu²⁺ were added into the electrolyte during the preparation of Cu-doped SnS thin films to adjust the content of Cu. Other deposition parameters, such as the contents of SnCl₂ and Na₂S₂O₃, deposition temperature and time were kept unchanged. The compositions of the Cu-doped SnS films were examined with EDX, and the results are listed in Table 3. It can be seen that the atomic ratio (Cu+Sn):S of the thin films at all Cu²⁺ contents is quite closed to the stoichiometric ratio of 1:1. The Cu content increased with the increase of the Cu²⁺ content of the electrolyte, so it can be easily controlled by the adjustment of the Cu²⁺ content of the electrolyte.

The SEM images of the thin films are shown in Fig. 3. It can be seen that the SnS thin film is compact and composed by homogeneous particles (Fig. 3a). After the Cu-doping, the compact and homogeneous morphology kept unchanged (Fig. 3b–e) [36]. In other words, Cu-doping did not influence the morphology of the SnS thin films. The thickness

of the Cu-doped SnS thin film with 0.62-at.% Cu was about 1.11 μm (Fig. 3f), and those of other thin films almost kept such value. XRD analysis indicated that the crystal structure of all Cu-doped SnS thin films kept orthogonal type. Such composition, crystal structure and morphology of the Cu-doped SnS thin films are advantageous for the thermoelectric performances.

Hall test indicated that all our samples of SnS and Cu-doped SnS are p-type semiconductor, which is in well accordance with the existing reports [22, 37]. The Hall test results of the Cu-doped thin films with different Cu contents are shown in Fig. 4. The E_g results of the SnS and Cu-doped SnS thin films are also shown in Fig. 4. It can be seen that all the carrier concentration (Fig. 4a), carrier mobility (Fig. 4b) and electrical resistivity (Fig. 4c) of the thin films fluctuated with the change of Cu content of the films. After the Cu-doping, the carrier concentration of all doped thin films increased, which is in well accordance with our expectation. The carrier concentration reached the maximum value at the Cu content of 0.62-at.%, which supported its minimum resistivity in spite of the minimum carrier mobility. The high carrier concentration of the Cu doped thin films should be caused by the narrowed band gap which is shown in Fig. 4d. The E_g of pure SnS thin film was 1.31 eV which is close to the reported value [38, 39]. The value was narrowed to 0.97 eV after 0.62-at.% Cu-doping, which is also close to the reported value of the E_g of the Cu-doped SnS [40, 41]. The

Table 3 EDX results of Cu-doped SnS thin films deposited in electrolytes with different Cu²⁺ contents

Cu ²⁺ content (mM)	Composition (at.%)			Atomic ratio (Cu+Sn):S
	Cu	Sn	S	
0.00625	0.62 ± 0.19	51.07 ± 2.02	48.31 ± 1.75	1:0.93
0.0125	0.99 ± 0.26	50.93 ± 1.88	48.08 ± 1.91	1:0.92
0.025	1.58 ± 0.42	51.03 ± 1.31	47.39 ± 1.58	1:0.90
0.05	2.01 ± 0.61	50.82 ± 1.66	46.17 ± 1.64	1:0.89

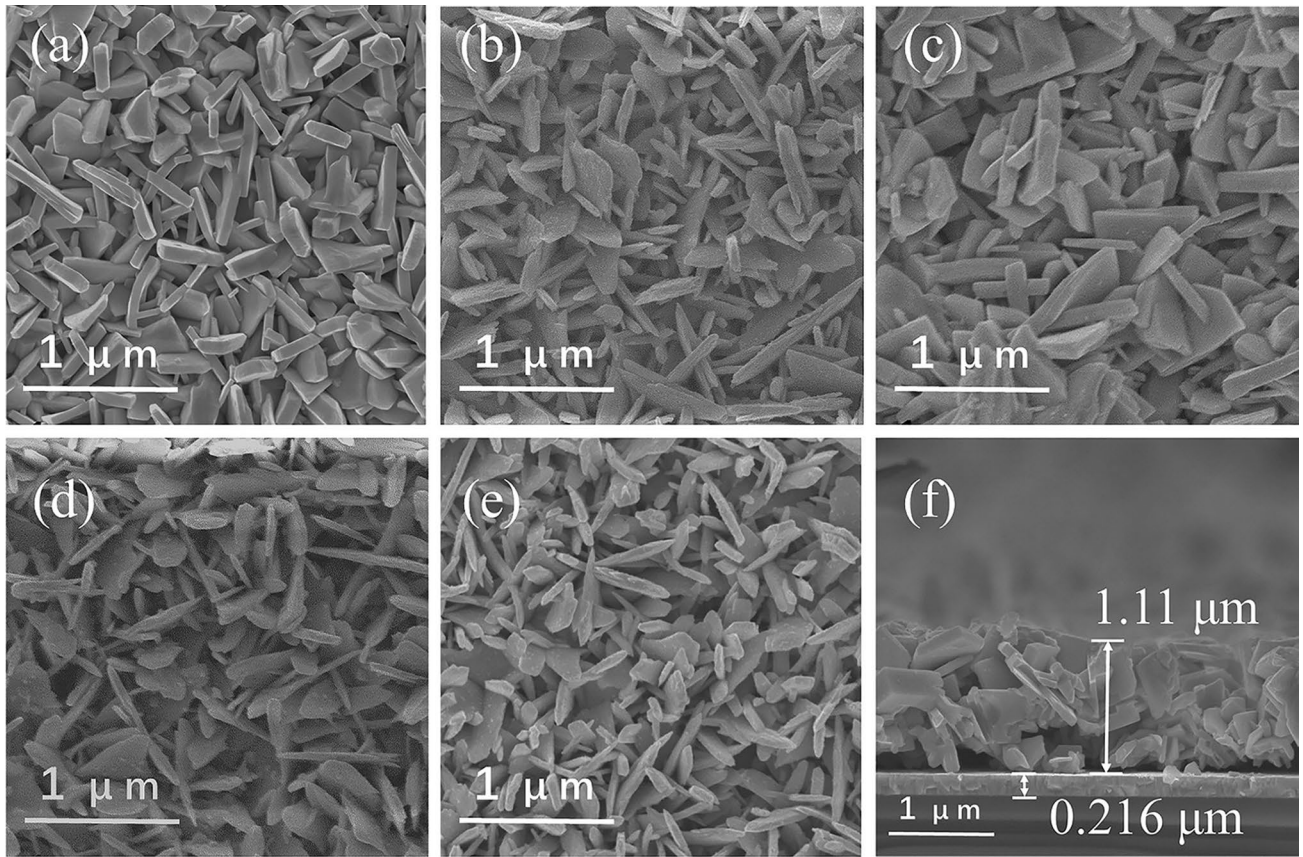
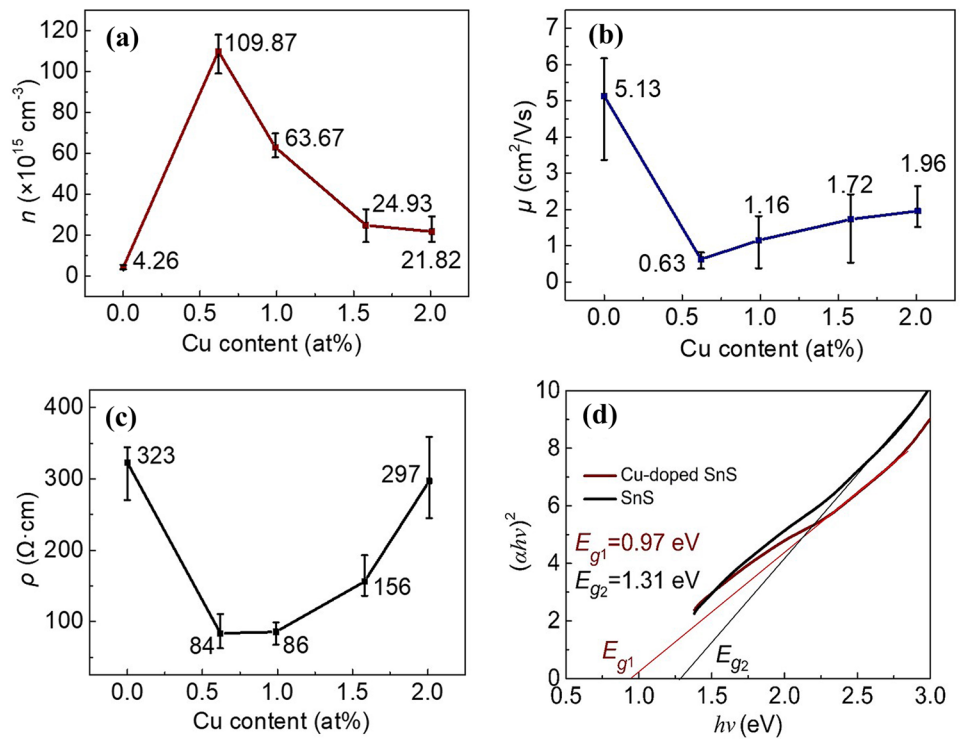


Fig. 3 SEM images of SnS and Cu-doped SnS thin films: **a** SnS without Cu doping; **b** Cu-doped SnS thin film with 0.62-at.% Cu; **c** Cu-doped SnS thin film with 0.99-at.% Cu; **d** Cu-doped SnS thin film with 1.58-at.% Cu; **e** Cu-doped SnS thin film with 2.01-at.% Cu; and **f** cross sectional image of Cu-doped SnS thin film with 0.62-at.% Cu

Fig. 4 Electrical performance of Cu-doped SnS thin films: **a** carrier concentration; **b** carrier mobility; **c** electric resistivity; and **d** band gaps of SnS and Cu-doped SnS thin films with 0.62 at.% Cu



results clearly indicate that Cu doping narrowed the band gap. The reason should be that Cu atoms provide an acceptor level to reduce the band gap of SnS, so that they accept electrons easier to form holes and promote the generation of carrier excitation. It should also be explained that the carrier concentration decreased when the Cu content was higher than 0.62-at.%. In fact, secondary phases other than orthorhombic SnS might appear when Cu content was too high [42], although they might not be observed by XRD because of the too low amount. Cu atoms might segregate in the secondary phases and decrease the actual Cu content in orthorhombic SnS. The carrier concentration therefore decreased when the Cu content increased.

It should be noticed that the resistivity of the thin films with 0.99-at.% Cu was also quite small, because the carrier concentration and mobility were both large. Therefore, the resistivity of the Cu-doped thin film could keep small in a wide Cu content range, which is profitable for the thermoelectric performance enhancement. The highest carrier concentration of Cu-doped SnS thin films reached $109.87 \times 10^{15} \text{ cm}^{-3}$ which is 25.79 times as large as that of the SnS thin films. And the lowest resistivity is only $84 \Omega \text{ cm}$ which is only 26% of that of the SnS thin films. Therefore, Cu-doping is a quite effective method to improve the carrier concentration and conductivity of SnS thin films. Such improvements can effectively promote the thermoelectric properties of SnS.

3.3 Texture control of Cu-doped SnS films

Considering the additives and their content in the electrolytes for pure SnS thin films (Fig. 1), different amount of additives of urea or CTAB was added into the plating bath to induce preferential growth of doped SnS thin films. The composition of the Cu-doped SnS thin films deposited in such conditions are shown in Table 4. It can be seen the Cu content of the doped SnS thin films always increased with the increase of the content of the additives. So the composition of the films should be controlled by the contents of both Cu^{2+} and the additives in these conditions. However, the Cu content of the doped SnS thin films were still in a reasonable range which could assure a high carrier concentration after the addition of the additives.

The SEM images of the pure and Cu-doped SnS thin films with and without additives are shown in Fig. 5. It can be seen that all the SnS thin films were composed by particles with different shapes. And all of the SnS thin films were homogeneous and compact. After the addition of the additives, the compact and homogeneous morphology of the SnS thin films kept unchanged. Such compact structure could assure their good carrier transmission characters.

The XRD spectra of the Cu doped SnS thin films with and without additives are shown in Fig. 6. All the

Table 4 EDX results of Cu-doped SnS films with and without additives

Additives	Composition (at.%)			Atomic ratio (Sn+Cu):S
	Cu	Sn	S	
0	0.62 ± 0.19	51.07 ± 2.02	48.31 ± 1.75	1:0.93
CTAB, 5 mg/L	0.85 ± 0.37	51.84 ± 1.97	47.32 ± 1.97	1:0.90
CTAB, 10 mg/L	1.04 ± 0.54	51.80 ± 2.08	47.16 ± 2.07	1:0.89
Urea, 5 mg/L	0.79 ± 0.20	51.39 ± 1.25	47.83 ± 1.26	1:0.92
Urea, 10 mg/L	1.07 ± 0.44	52.40 ± 2.72	46.53 ± 1.43	1:0.87

diffraction peaks corresponding well with the standard card of orthorhombic SnS (JCPDS 39-0354) except those belong to ITO substrate. The texture coefficients of all Cu-doped SnS thin films with and without additives were calculated with formula (1) and are listed in Table 5. The texture coefficients of pure SnS films with and without additives are also listed in Table 5 for comparison.

It can be seen that almost all the thin films had the texture of (200) or (040). The texture coefficient of (040) of the SnS thin films without additives increased from 1.67 to 2.91 after Cu-doping. After the adding of urea, the texture coefficient of (040) of the SnS thin films increased obviously. It increased from 1.67 to 2.73 for pure SnS thin films and from 2.91 to 3.85 for the Cu-doped ones. The adding of urea promoted the (040) growth more for the Cu-doped SnS thin films, so the largest value of texture coefficient of (040) reached 3.85 which was much larger than that of pure SnS films of 2.73. After the adding of CTAB, the strong texture of both the pure and doped SnS thin films changed into (200). On this condition, the largest value of the texture coefficient of (200) of the doped SnS films of 3.93 of was still much larger than that of pure SnS films of 2.32. All these results indicated that the additives had stronger influence on the preferential growth of the doped SnS films than that on the pure SnS films. Compared with the pure SnS thin films, the texture coefficient of the doped films can be adjusted by additives more effectively.

3.4 Influence of texture on electrical properties

Hall test results of pure and Cu-doped SnS thin films with different texture are shown in Table 6. As analyzed above, the carrier concentration of the SnS thin films increased greatly after Cu-doping. However, the carrier mobility decreased obvious after the Cu doping simultaneously. The orientation and coefficient of the textures of the thin films influenced the carrier mobility obviously. For instance, the texture coefficient of (040) of both the pure and Cu-doped

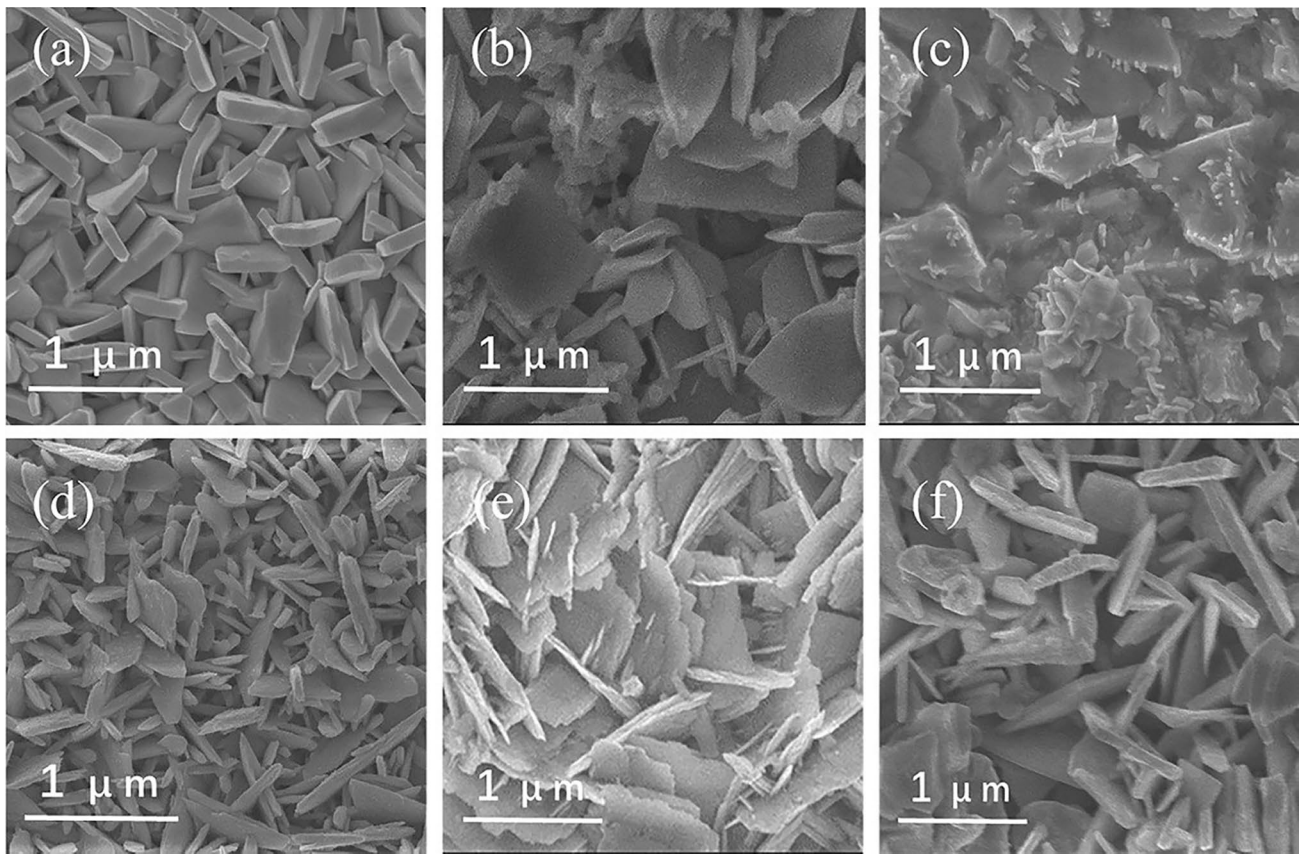


Fig. 5 SEM images of the pure and doped SnS thin films with and without additives: **a** pure SnS without additive; **b** pure SnS with CTAB; **c** pure SnS with urea; **d** additive-free Cu-doped SnS; **e** Cu-doped SnS with CTAB; **f** Cu-doped SnS with urea

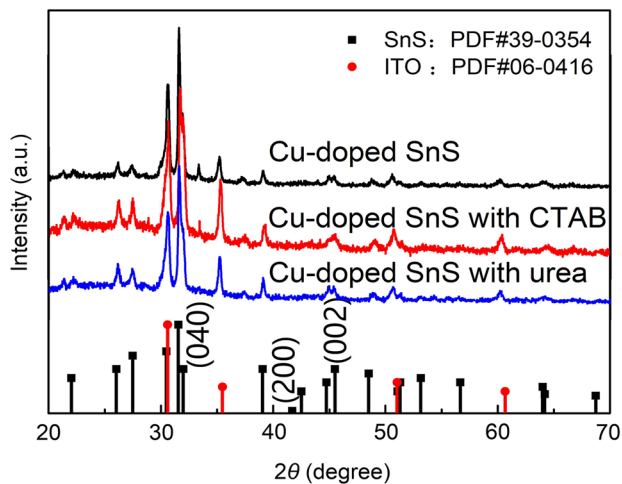


Fig. 6 XRD spectra of the Cu-doped SnS films with and without additives

SnS thin films increased after the adding of urea, and their carrier mobilities of the thin films decreased meanwhile. It indicates that the (040) texture is disadvantageous for the promotion of carrier mobilities of such thin films. On the

Table 5 Texture coefficient of pure and Cu-doped SnS thin films with and without additives

Thin film	Additive	Additive content (mg/L)	T_{200}	T_{040}	Strong texture
SnS	–	–	1.00	1.67	(040)
SnS	CTAB	10	2.32	2.14	(200)
SnS	Urea	10	1.77	2.73	(040)
0.62%Cu–SnS	–	–	1.57	2.91	(040)
0.85%Cu–SnS	CTAB	5	3.93	2.83	(200)
0.79%Cu–SnS	Urea	5	3.16	3.85	(040)

other hand, the orientation of texture changed into (200) after the adding of CTAB, the carrier mobilities of both the pure and Cu-doped SnS thin films increased obviously. It should be noticed that it increase from 0.63 to 1.94 $\text{cm}^2/\text{V s}$ for Cu-doped SnS films (Table 6), which is an 308% increment. So the carrier mobility can be effectively adjusted by texture control. Supported by such a carrier mobility increment, the electric resistivity of the Cu-doped SnS thin film decreased from 83.53 to 24.50 $\Omega \text{ cm}$. Compared with the SnS thin film without Cu-doping and texture adjustment,

Table 6 Electrical performance of pure and Cu-doped SnS thin films with different texture

Thin films	Additive	Texture	T_{hkl}	n ($\times 10^{15}$ cm $^{-3}$)	μ (cm 2 /V s)	ρ (Ω cm)
SnS	–	(040)	1.67	4.26	5.13	323.22
SnS	CTAB	(200)	2.32	6.12	7.44	174.21
SnS	Urea	(040)	2.73	12.69	0.77	700.48
0.62%Cu–SnS	–	(040)	2.91	109.87	0.63	83.53
0.85%Cu–SnS	CTAB	(200)	3.93	171.72	1.94	24.50
0.79%Cu–SnS	Urea	(040)	3.85	436.42	0.32	50.21

the resistivity of the Cu-doped thin film with (200) texture decreased from 322.53 to 24.50 Ω cm, which is a delightful improvement.

It should be noticed that the carrier concentration of the SnS films was obviously increased by Cu-doping through the change of the band gap, and the carrier mobility of the thin films was successfully increased by the adjustment of texture through additives. Such increments effectively decreased the electric resistivity of SnS thin films which has obvious advantages for the enhancement of its thermoelectric performance. So our results provide a new view to improve the electric transmission performance of thermoelectric thin films.

4 Conclusions

Cu-doped SnS films were electrodeposited by potentiostatic methods. The Cu content of the thin films were controlled by the adjustment of the Cu content in the electrolyte. The doping of Cu narrowed the band gap of the SnS thin film to cause more carriers. So the carrier concentration of the SnS thin films can be effectively increased by the Cu-doping. The largest carrier concentration increased from 4.26×10^{15} to 436.42×10^{15} cm $^{-3}$ after Cu doping. By the additives in the electrolyte, the texture orientation and its coefficient were successfully controlled. The addition of urea could increase the texture coefficient of (040), and the addition of CTAB could cause (200) texture. The carrier mobility of both the pure and Cu-doped SnS thin films had close relation to the texture orientation and their coefficient. The carrier mobility of the Cu-doped SnS thin films increased from 0.63 to 1.94 cm 2 /V s by the (200) texture, so the (200) texture could effectively increase the carrier mobility. With a sample electrodeposition method, we successfully accomplished the combination of the Cu-doping and texture control of SnS thin films. By such a combination, the resistivity of the Cu-doped thin film with (200) texture decreased from 322.53 to 24.50 Ω cm, so the combination was an effective path to improve the electric transmission performance of SnS thin films. Our results provide an easy method and a new view to improve the electric transmission performance of thermoelectric thin films.

Acknowledgements This work was supported by the National Natural Science Foundation of China (Grant No. 51472020).

References

1. C. Gao, G. Chen, *Compos. Sci. Technol.* **124**, 52–70 (2016)
2. L.D. Zhao, S.H. Lo, Y. Zhang, H. Sun, G. Tan, C. Uher, C. Wolverton, V.P. Dravid, M.G. Kanatzidis, *Nature* **508**, 7496 (2014)
3. L.D. Zhao, G. Tan, S. Hao, J. He, Y. Pei, *Science* **351**, 141–144 (2017)
4. A.J. Minnich, M.S. Dresselhaus, Z.F. Ren, G. Chen, *Energy Environ. Sci.* **2**, 5 (2009)
5. Y. Kumagai, L.A. Burton, A. Walsh, F. Oba, *Phys. Rev. Appl.* **6**, 1 (2016)
6. R. Guo, X. Wang, Y. Kuang, B. Huang, *Phys. Rev. B* **92**, 115 (2015)
7. T.M. Tritt, *Science* **283**, 5403 (1999)
8. J. Yang, L. Xi, W. Qiu, L. Wu, X. Shi, L. Chen, J. Yang, W. Zhang, C. Uher, D.J. Singh, *NPJ Comput. Mater.* **2**, 1 (2016)
9. T. Gotoh, *Phys. Status Solidi A* **213**, 7 (2016)
10. B.Z. Sun, Z. Ma, C. He, K. Wu, *RSC Adv.* **5**, 69 (2015)
11. Q. Tan, C.F. Wu, W. Sun, J.F. Li, *RSC Adv.* **6**, 50 (2016)
12. H.-S. Kim, Z.M. Gibbs, Y. Tang, H. Wang, G.J. Snyder, *APL Mater.* **3**, 4 (2015)
13. D.M. Unuchak, K. Bente, V.A. Ivanov, V.F. Gremenok, *Cryst. Res. Technol.* **45**, 11 (2010)
14. N.K. Singh, S. Bathula, B. Gahtori, K. Tyagi, D. Haranath, A. Dhar, *J. Alloys Comp.* **668**, 152–158 (2016)
15. E.K. Chere, Q. Zhang, K. Dahal, F. Cao, J. Mao, Z. Ren, *J. Mater. Chem. A* **4**, 5 (2016)
16. Y. Goto, F. Naito, R. Sato, K. Yoshiyasu, T. Itoh, Y. Kamihara, M. Matoba, *Inorg. Chem.* **52**, 17 (2013)
17. V. Steinmann, R.E. Brandt, R. Chakraborty, R. Jaramillo, M. Young, B.K. Ofori-Okai, C. Yang, A. Polizzotti, K.A. Nelson, R.G. Gordon, T. Buonassisi, *APL Mater.* **4**, 2 (2016)
18. M. Abdullah Almessiere, A.L. Al-Otaibi, I.B. Assaker, T. Ghrib, R. Chtourou, *Mater. Sci. Semicond. Process.* **40**, 873–878 (2015)
19. Y. Yang, S. Cheng, *J. Semicond.* **29**, 12 (2008)
20. O. Falkenbach, J. Tinz, A.S. Schulze, E. Mueller, S. Schlecht, *Phys. Status Solidi A* **213**, 3 (2016)
21. C. Bera, S. Jacob, I. Opahle, N.S. Gunda, R. Chmielowski, G. Dennler, G.K. Madsen, *Phys. Chem. Chem. Phys.* **16**, 37 (2014)
22. S. Bhattacharya, N.S. Gunda, R. Stern, S. Jacobs, R. Chmielowski, G. Dennler, G.K. Madsen, *Phys. Chem. Chem. Phys.* **17**, 14 (2015)
23. M. Patel, A. Ray, *RSC Adv.* **4**, 74 (2014)
24. J. Xia, X.Z. Li, X. Huang, N. Mao, D.D. Zhu, L. Wang, H. Xu, X.M. Meng, *Nanoscale* **8**, 4 (2016)
25. H. Zhang, Y. Balaji, A. Nalin Mehta, M. Heyns, M. Caymax, I. Radu, W. Vandervorst, A. Delabie, *J. Mater. Chem. C* **6**(23), 6172–6178 (2018)

26. J. Sun, Y. Huang, S. Nie, Z. Chen, J. Xu, L. Zhao, W. Zhou, Q. Wang, H. Gong, *Mater. Lett.* **178**, 171–174 (2016)
27. Y. Kawano, J. Chantana, T. Minemoto, *Curr. Appl. Phys.* **15**, 8 (2015)
28. B. Ghosh, R. Roy, S. Chowdhury, P. Banerjee, S. Das, *Appl. Surf. Sci.* **256**, 13 (2010)
29. A. Kassim, H.S. Min, W.T. Tan, M.J. Haron, *J. Appl. Sci. Res.* **4**, 12 (2008)
30. Y. Liu, D. Hou, G. Wang, *Chem. Phys. Lett.* **379**, 1–2 (2003)
31. P.K.D. Gupta, S.P. Moulik, *Colloid Polym. Sci.* **267**, 3 (1989)
32. Z. Tian, C. Guo, M. Zhao, R. Li, J. Xue, *ACS Nano* **11**, 11368–11375 (2017)
33. A. Shafique, Y.H. Shin, *Sci. Rep.* **7**, 1 (2017)
34. H. Kafashan, F. Jamali-Sheini, R. Ebrahimi-Kahrizsangi, R. Yousefi, *J. Alloys Comp.* **681**, 595–605 (2016)
35. A.A. Ramadan, A.A. Abd El-Mongy, A.M. El-Shabiny, A.T. Mater, S.H. Mostafa, E.A. El-Sheheedy, H.M. Hashem, *Cryst. Res. Technol.* **44**, 111 (2009)
36. S.A. Bashkirov, V.F. Gremenok, V.A. Ivanov, V.V. Shevtsova, P.P. Gladyshev, *Thin Solid Films* **585**, 40–44 (2015)
37. B. Ghosh, M. Das, P. Banerjee, S. Das, *Solid State Sci.* **11**, 2 (2009)
38. P.D. Antunez, D.A. Torelli, F. Yang, F.A. Rabuffetti, N.S. Lewis, R.L. Brutchey, *Chem. Mater.* **26**, 19 (2014)
39. J. Xu, Y. Yang, Z. Xie, *J. Mater. Sci.: Mater. Electron.* **25**, 7 (2014)
40. G.G. Ninan, C. Sudha Kartha, K.P. Vijayakumar, *Sol. Energy Mater. Sol. Cells* **157**(229), 233 (2016)
41. N.R. Mathews, J. Tamy Benítez, F. Paraguay-Delgado, M. Pal, L. Huerta, *J. Mater. Sci.: Mater. Electron.* **24**, 10 (2013)
42. S. Nakamura, H. Funabiki, S. Shiga, *Phys. Status Solidi C* **14**, 6 (2017)

Publisher's Note Springer Nature remains neutral with regard to jurisdictional claims in published maps and institutional affiliations.